JMEPEG (2017) 26:3977–3982
DOI: 10.1007/s11665-017-2852-y

1059-9495/$19.00

Microstructures and Mechanical Properties of Binary Al-Zn Alloys Fabricated by Casting and Heat Treatment

W.B. Zhou, G.B. Teng, C.Y. Liu, H.Q. Qi, H.F. Huang, Y. Chen, and H.J. Jiang

(Submitted November 14, 2016; in revised form June 6, 2017; published online August 4, 2017)

Binary Al-Zn alloys with different Zn contents were fabricated by casting and heat treatment. Analysis of mechanical properties showed that the hardness and tensile strength of Al-Zn alloys increased with increased Zn content, with the post-heat treatment hardness and ultimate tensile strength of Al-49Zn alloy reaching as high as 152 HV and 330 MPa, respectively. Meanwhile, the plasticity and toughness of Al-Zn alloys decreased with increased Zn content. Solid-solution strengthening was the main strengthening mechanism for Al-Zn alloys, and Orowan strengthening was also observed in Al-49Zn alloy. The fracture mode of Al-20Zn and Al-35Zn alloys was ductile, whereas Al-20Zn alloy showed good impact toughness. This work provided a basis for further improving the cast component design of the Al-Zn-X system.

Keywords Al alloy, heat treatment, mechanical properties microstructures

1. Introduction

Al alloys are receiving considerable attention for structural applications due to their low production cost, high liquid flow capacity, and good thermal stability (Ref 1-5). To date, Al-Si base is the most commonly used system for cast Al alloys (Ref 6, 7). The tensile strength and hardness of Al-Si base alloys are known to be very low in their as-cast state. Thus, to improve the mechanical properties of Al-Si base cast alloys, artificial aging after solid-solution treatment that can precipitate the nanoscale phase and achieve precipitation strengthening must be used in these alloys (Ref 8, 9).

Heat treatment without subsequent artificial aging can significantly reduce the production cost and improve the production efficiency of cast Al alloys. Thus, the development of new cast Al alloy systems not requiring artificial aging has potential engineering applications.

As shown in the Al-Zn phase diagram in Fig. 1, a high number of Zn atoms can be dissolved in the Al lattice within a wide temperature range (Ref 10), and serious lattice distortion in Al-Zn alloy can lead to solid-solution strengthening of this alloy (Ref 11-14). Furthermore, no intermetallic compound was observed between Al and Zn, so solid-solution strengthening was the main strengthening mechanism in Al-Zn alloy and single solid-solution treatment can be used as heat treatment method of Al-Zn alloy. Apart from saving on the artificial aging process, the low melting points of Al-Zn alloys led to other cost benefits, such as the extension of die life and energy savings from melting (Ref 15).

W.B. Zhou, Alnan Aluminium Co., Ltd., Nanning 530031, China; and **G.B. Teng, C.Y. Liu, H.Q. Qi, H.F. Huang, Y. Chen,** and **H.J. Jiang**, Key Laboratory of New Processing Technology for Nonferrous Metal and Materials, Ministry of Education, Guilin University of Technology, Guilin 541004, China. Contact e-mails: lcy261@glut.edu.cn and jhj@glut.edu.cn.

Our previous works have shown that binary Al-20 wt.% Zn alloy possesses excellent strength and plasticity (Ref 16-21). Increasing the Zn contents of Al-Zn alloy must lead to more serious lattice distortion of Al matrix, which can cause higher hardness and tensile strength. However, systematic studies on the microstructures and mechanical properties of high-Zn-content binary Al-Zn alloys during casting and heat treatment processes are lacking.

In the present study, high-Zn-content binary Al-Zn alloys with different Zn contents were fabricated by melting and casting. To optimize the performance of Al-Zn alloys, they were subjected to solid-solution treatment with different parameters. We aimed to (a) clearly understand the solidification and solid-solution process of the Al-Zn system, (b) elucidate the influence of Zn content on the microstructure, mechanical properties, and deformation mechanism of Al-Zn alloys, and (c) obtain new cast Al alloy systems with cost benefits and thus provide a basis for improving the further cast component design of the Al-Zn-X system.

2. Experimental Methods

Al-20Zn, Al-35Zn, and Al-49Zn (mass fraction) alloys were prepared by melting commercial pure Al (99.9%) and pure Zn (99.9%) in a resistance heating furnace with a graphite crucible. A graphite casting mold was used, and the casting temperatures of Al-20Zn, Al-35Zn, and Al-49Zn alloys were 983, 953, and 923 K, respectively. The as-cast alloys were heated for 5 h and then quenched in water. Heat treatment was conducted from 573 to 803 K, and different temperatures were employed for different Al-Zn alloys according to their melting points.

The microstructures of alloys were examined by optical microscopy (OM), scanning electron microscopy (SEM), and transmission electron microscopy (TEM). The grain size and arm spacing for samples were measured by the intercept method. The chemical (Al and Zn elements) composition of SEM specimens was examined by energy-dispersive x-ray spectrometry (EDS). TEM films were prepared by grinding the alloy to a thickness of 30 μm followed by ion milling. The

phases of Al-Zn alloys after each different treatment were confirmed by x-ray diffraction (XRD) with Cu Ka radiation.

Hardness measurements were performed with a Vickers microhardness tester (using 3000 gf load for 15 s). Hardness tests on every sample were repeated ten times to check the reproducibility and reliability of results. Tensile tests were performed at a strain rate of 1×10^{-4} s^{-1} by using an Instron 5982-type test machine. The surfaces after the tensile tests were observed by SEM. Charpy impact tests with a pendulum were carried out to evaluate the impact toughness of the Al-Zn alloys. Standard 2-mm Charpy V-notch samples with dimensions of $10 \times 10 \times 55$ mm^3 were machined in the crack arrester orientation.

3. Results and Discussion

Figure 2 shows the OM images of as-cast Al-Zn alloys with different Zn contents. A typical dendritic structure was observed in the as-cast alloys, and arm spacing decreased with increased Zn contents. A structure with an average arm spacing of about 20 μm was obtained in the as-cast Al-49Zn alloy, as shown in Fig. 2(c).

The microstructure of as-cast Al-49Zn alloy was also examined by SEM and TEM (Fig. 3). Figure 3(a) and (b) shows that a high concentration of Zn gathered in the interdendritic eutectic regions of the as-cast alloy due to the segregation of solutes during casting. The white and gray regions in the TEM image corresponded with Al and Zn phases, respectively. A high density of nanoscale Zn lamellae was observed in coarse Al grains, as shown in Fig. 3(c).

A typical eutectic growth model was observed in the Al-Zn system during solidification. The growth of Al-rich crystal resulted in the accumulation of Zn atoms near the Al phase, and the enrichment of Zn atoms promoted the nucleation and growth of the Zn phase in the neighboring regions of Al crystal. Thus, Zn fibers and lamellae were observed in the Al grains (Fig. 3c).

Figure 4 shows the OM images of as-SS Al-Zn alloys with different Zn contents. All three samples showed a similar grain structure. The dendritic grains disappeared, and equiaxed grains about 200 μm in size were obtained in the as-SS Al-Zn alloys.

The element distribution of as-SS Al-49Zn alloy was examined by SEM and EDS (Fig. 5). Compared with as-cast Al-49Zn alloy, recrystallization and grain coarsening of Al were obtained in the Al-49Zn alloy after heat treatment at 673 K for 5 h (Fig. 3a and 5a). Furthermore, GB segregation of Zn in as-cast Al-49Zn alloy was eliminated in Al-Zn alloys after solid-solution treatments (Fig. 3b and 5b).

Figure 6 shows the TEM images of as-SS Al-Zn alloys with different Zn contents. Al-20Zn alloy was characterized by the absence of Zn precipitate phase and well-defined GBs, as shown in Fig. 6(a). Figure 6(b) shows that an equiaxed Zn phase about 500 nm in size was obtained along the GBs in as-SS Al-35Zn alloy. The low density of Zn phase in Al-20Zn and Al-35Zn alloys meant that most Zn atoms dissolved in the Al lattice during heat treatment and were then frozen in the Al matrix during water quenching. Hence, a solid-solution reaction occurred in Al-Zn alloys.

Compared with the grain interior Zn phase in as-cast Al-49Zn alloy, the grain interior Zn phase in as-SS Al-49Zn alloy showed a similar shape but smaller size and more uniform distribution in Al matrix, as shown in Fig. 6(c).

Figure 7 shows the XRD patterns of as-cast and as-SS Al-Zn alloys. The Zn peak was not observed in as-SS Al-20Zn alloy, but obvious Zn peaks and nearly no change in intensity were observed in Al-49Zn alloy after solid-solution treatment. These findings corresponded well with the TEM images (Fig. 6a and c). The Al peaks obviously shifted toward the high-angle orientation after heat treatment, as shown in the inset in Fig. 7.

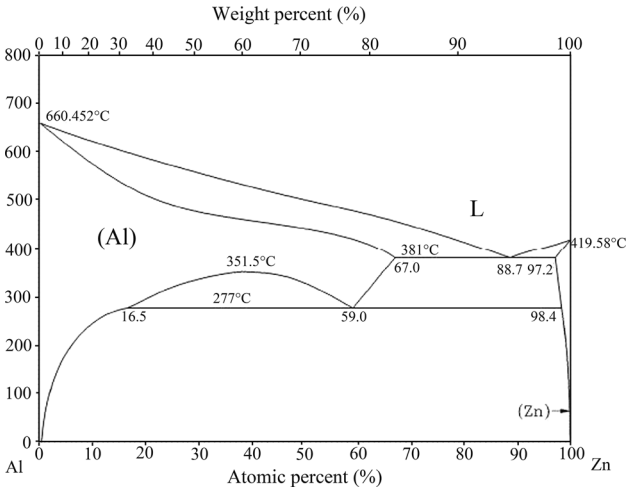

Fig. 1 Al-Zn binary phase diagram (Ref 10)

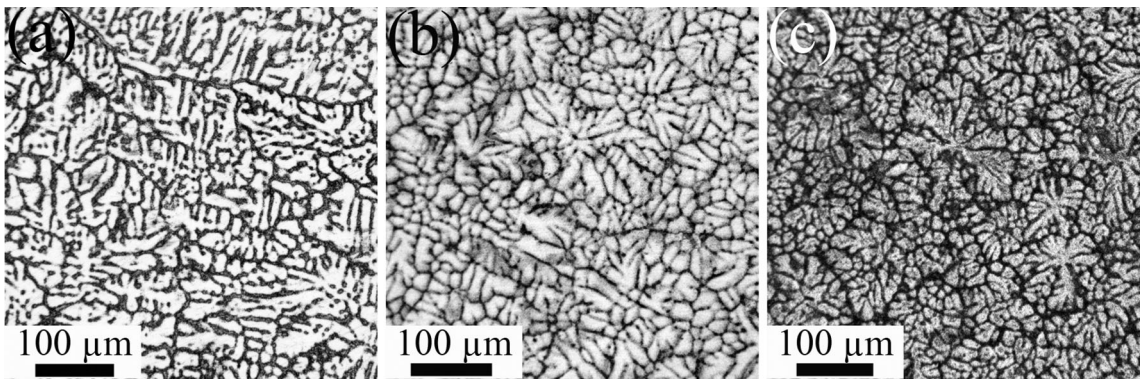

Fig. 2 OM images of as-cast (a) Al-20Zn, (b) Al-35Zn, and (c) Al-49Zn alloys

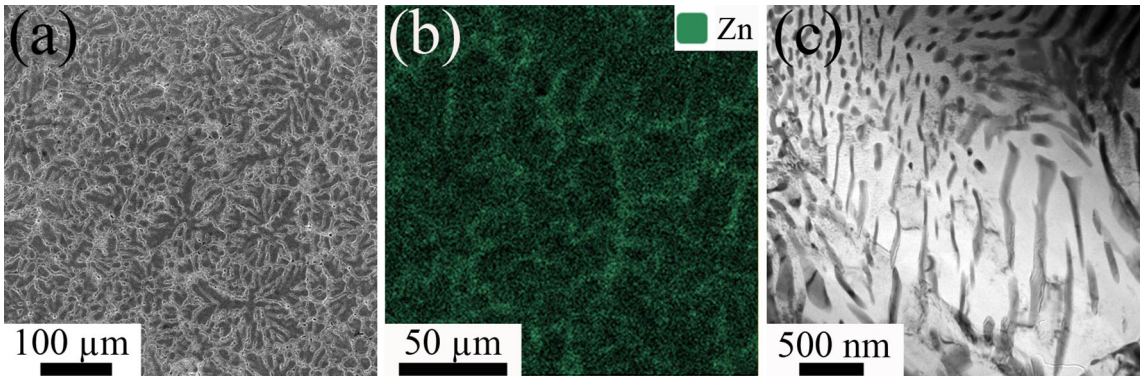

Fig. 3 (a) SEM image, (b) EDS map of Zn element, and (c) TEM image of as-cast Al-49Zn alloy

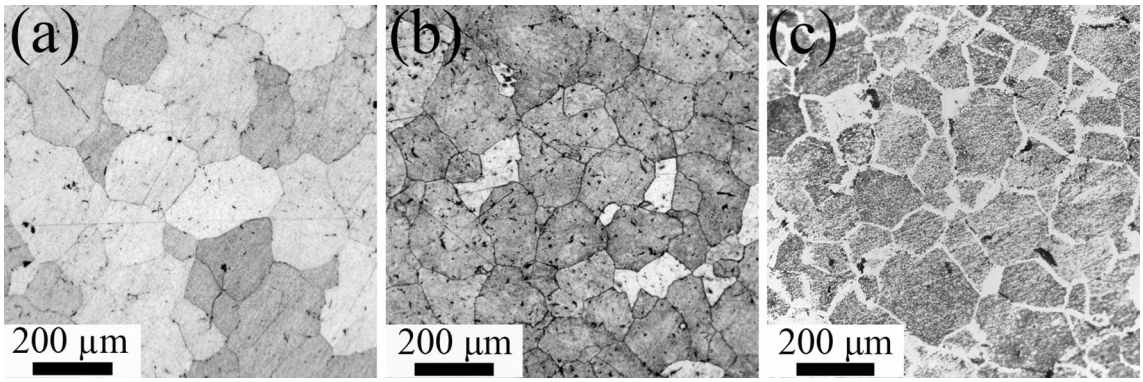

Fig. 4 OM images of (a) as-SS Al-20Zn alloy treated at 530 °C for 5 h, (b) Al-35Zn alloy treated at 470 °C for 5 h, and (c) Al-49Zn alloy treated at 400 °C for 5 h

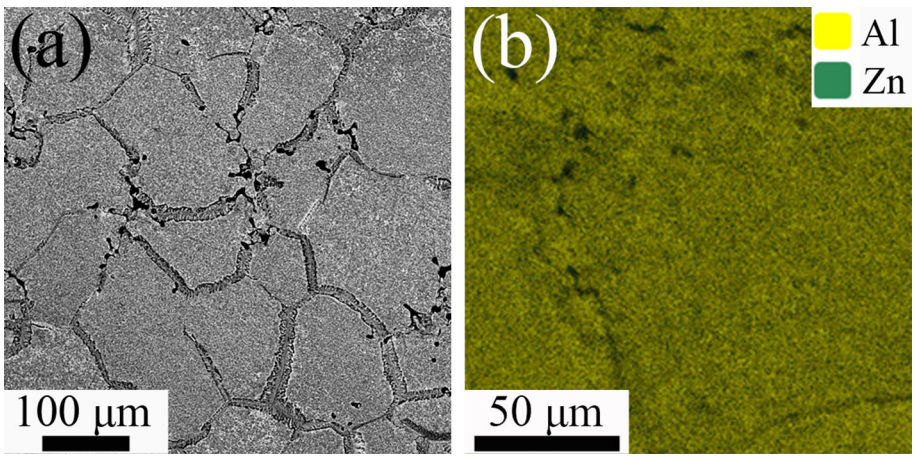

Fig. 5 (a) SEM image and (b) EDS map of Al-49Zn alloy treated at 400 °C for 5 h

Apart from the recrystallization and grain coarsening of Al, three phenomena were observed in Al-49Zn alloy during heat treatment: (1) The segregation of Zn was almost eliminated (Fig. 5b), (2) the size of the Zn phase in Al grains was obviously refined (Fig. 6c), and (3) the Al XRD peaks shifted toward the high-angle orientation (Fig. 7). Solid-solution reaction possibly led to the uniform distribution of Zn elements and the refinement of Zn phase. The atomic radius of Zn (0.153 nm) was smaller than that of Al (0.182 nm). As Zn atoms dissolved in Al lattice, the lattice parameter of Al matrix decreased, and the Al peaks shifted toward the high-angle orientation. Thus, an obvious solid-solution reaction occurred in the as-cast Al-49Zn alloy during heat treatment.

Figure 8 shows that the hardness of as-cast Al-Zn alloys increased with increased Zn content, and solid-solution treatment can effectively increase the hardness of Al-Zn alloys. After heat treatment at 673 K, as-SS Al-49Zn showed the highest hardness value of 152 HV. Moreover, as-SS Al-49Zn alloy showed higher hardness than Al-44Zn-2.5Cu (Ref 15) and Al-Si base alloys (Ref 22-24).

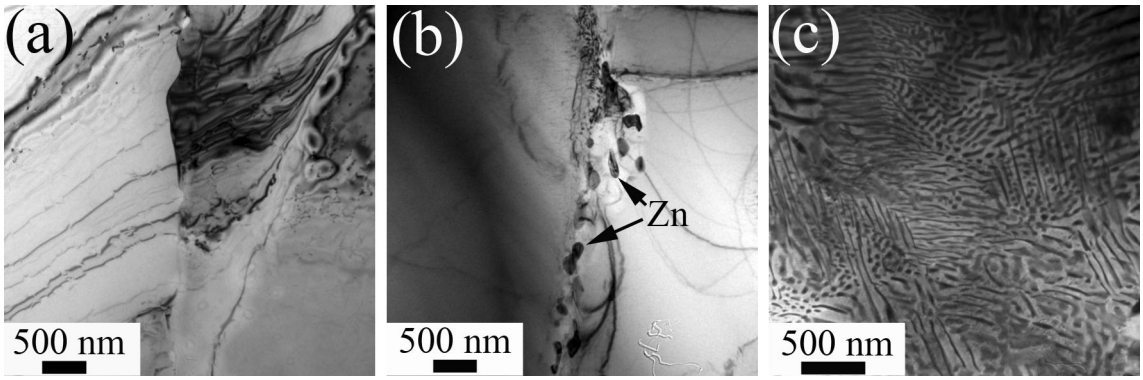

Fig. 6 TEM images of (a) as-SS Al-20Zn alloy treated at 530 °C for 5 h, (b) Al-35Zn alloy treated at 470 °C for 5 h, and (c) Al-49Zn alloy treated at 400 °C for 5 h

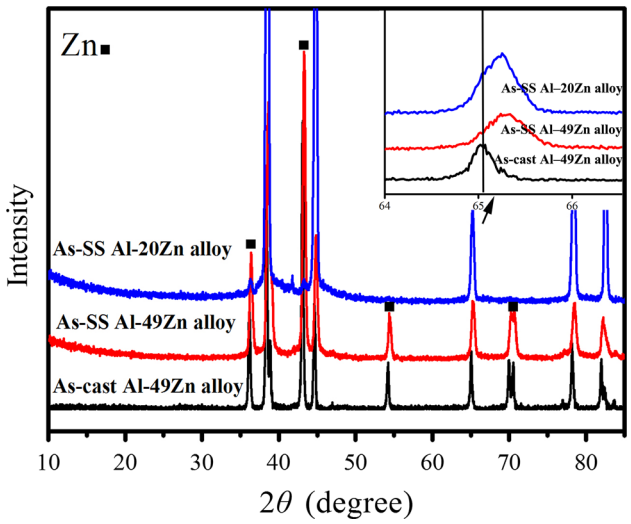

Fig. 7 XRD of as-cast Al-49Zn alloy, as-SS Al-20Zn, and Al-49Zn alloys treated at 803 and 673 K for 5 h

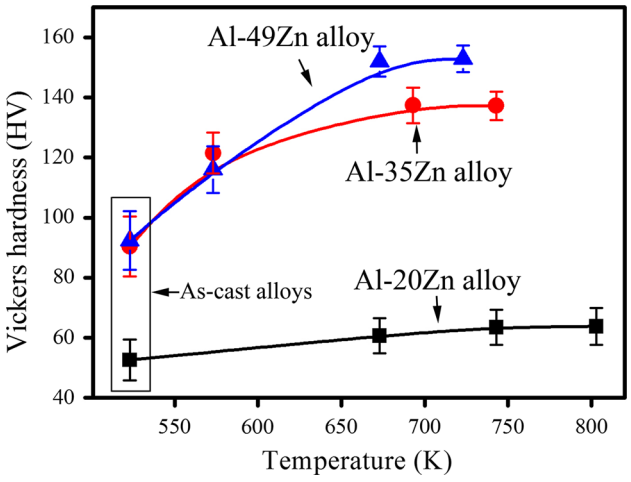

Fig. 8 Vickers hardness of as-cast and as-SS Al-Zn alloys after heat treatment at different temperatures for 5 h

Compared with as-cast Al-Zn alloys, as-SS Al-Zn alloy showed lower GB strengthening effect due to grain coarsening. However, the dissolution of Zn atoms into Al lattice increased

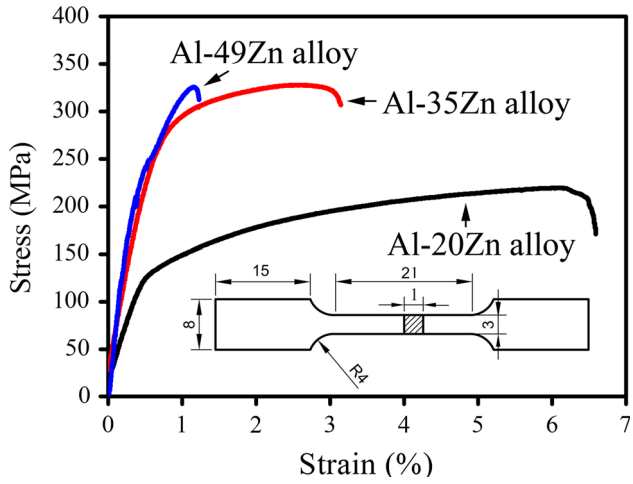

Fig. 9 Stress-strain curves of as-SS Al-Zn alloys

the solid solution of Al-Zn alloys. For as-SS Al-49Zn alloy, the Zn phase in Al grains was refined due to the solid-solution reaction; thus, Orowan strengthening by the nanoscale Zn phase was another important strengthening mechanism for as-SS Al-49Zn alloy. The net effect resulted in the hardening of as-SS Al-Zn alloys higher than that of as-cast Al-Zn alloys.

Figure 9 shows the stress-strain curves of as-SS Al-20Zn, Al-35Zn, and Al-49Zn alloys treated at 803, 743, and 673 K, respectively. The measurement error of strength and elongation values was $<3\%$. The lowest yield strength and ultimate strength were exhibited by as-SS Al-20Zn alloy. However, the tensile elongation of this sample was as high as 6.8%. Compared with as-SS Al-35Zn and Al-49Zn alloys, as-SS Al-20Zn alloy showed lower solubility and solid-solution strengthening effect and thus lower tensile strength. The lower solubility of as-SS Al-20Zn alloy also weakened the interaction between solute atoms and dislocation during tensile process. Hence, as-SS Al-20Zn alloy showed higher work hardening rate and elongation.

Different from the trend of change in hardness, as-SS Al-49Zn alloy did not show higher strength than Al-35Zn alloy during tensile process, as shown in Fig. 9. The serious lattice distortion in as-SS Al-49Zn alloy led to the plastic instability of this sample during tensile test, which decreased the strength and elongation values.

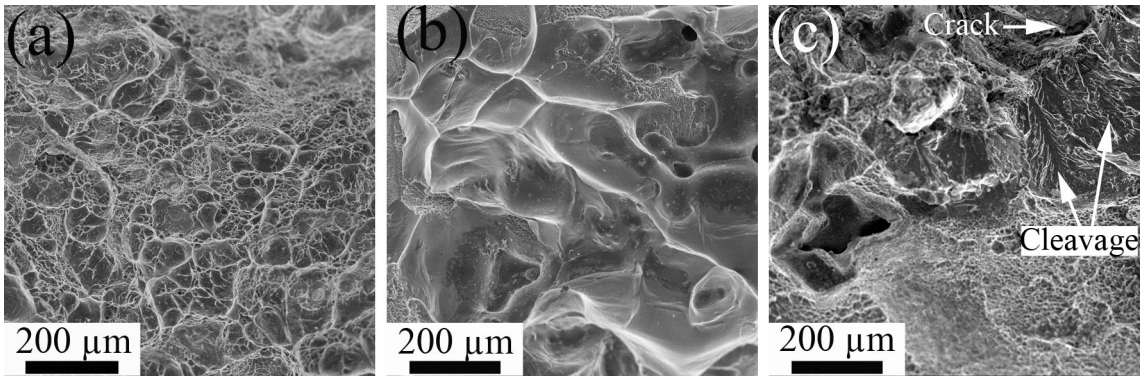

Fig. 10 SEM fractographs after tensile test: (a) as-SS Al-20Zn alloy treated at 803 K for 5 h, (b) Al-35Zn alloy treated at 743 K for 5 h, and (c) Al-49Zn alloy treated at 673 K for 5 h

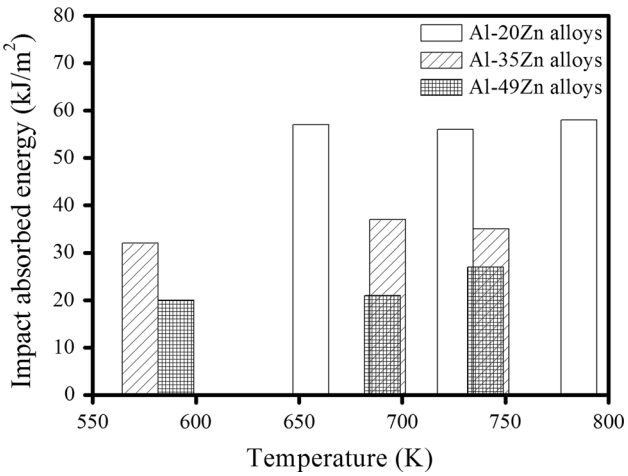

Fig. 11 Impact toughness of as-SS Al-Zn alloys after heat treatment at different temperatures for 5 h

SEM analysis was conducted to determine the rupture mechanisms of as-SS Al-Zn alloys. Fracture surfaces after tensile tests are shown in Fig. 10. Figure 10(a) and (b) revealed that as-SS Al-20Zn and Al-35Zn alloys exhibited ductile fractures with dimples and shear zones. The rupture model consisted of a fracture that occurred through the formation and coalescence of microvoids crossing the entire sample (Ref 25-27).

The fracture surface of as-SS Al-49Zn alloy illustrated the typical cleavage fracture type, as evidenced by many brittle cleavage planes separated by tearing ridges (Fig. 10c). Cracks can also be observed in this sample. The fracture surface characteristics of as-SS Al-49Zn alloy corresponded well with the poor ductility of this sample (Fig. 9).

Figure 11 shows that the impact toughness of as-SS Al-Zn alloys decreased with increased Zn content, whereas the temperature of solid-solution treatment was not very effective in influencing Charpy impact values. With increased Zn content of Al-Zn alloys, hardness and strength increased and ductility decreased. The impact values of metal were also influenced by both the ultimate tensile strength and the elongation due to fracture (Ref 28). The net effect of strength and ductility resulted in the highest impact toughness (58 kJ/m^2) of as-SS Al-20Zn alloy. Notably, as-SS Al-20Zn alloy showed similar impact toughness to traditional cast aluminum alloy, such as as-SS Al-Si base alloy (Ref 29).

4. Conclusion

The effects of Zn content on the microstructures and mechanical properties of binary Al-Zn alloys during casting and heat treatment processes were investigated. The following conclusions were drawn.

1. A typical dendritic structure was obtained in the as-cast Al-Zn alloys, and arm spacing decreased with increased Zn content. A typical eutectic growth model was exhibited in Al-Zn alloys during solidification, and Zn segregation occurred in the interdendritic eutectic regions after casting.
2. Solid-solution treatment induced a change in dendritic grains to equiaxed grains about 200 μm in size, a uniform distribution of Zn elements in Al-Zn alloys, and a refinement of the Zn phase in Al-49Zn alloy.
3. The hardness of Al-Zn alloys increased with increased Zn content, and the hardness of Al-49Zn alloy after heat treatment reached as high as 152 HV. Solid-solution strengthening was the main strengthening mechanism of as-SS Al-Zn alloys. Orowan strengthening by the nanoscale Zn phase was another strengthening mechanism of as-SS Al-49Zn alloy.
4. With increased Zn content in Al-Zn alloys, tensile strength increased and tensile elongation decreased. The ultimate tensile strength of Al-49Zn alloy was 330 MPa, and the tensile elongation of Al-20Zn alloy was 6.8%. The fracture mode of as-SS Al-20Zn and Al-35Zn alloys was ductile.
5. The impact toughness of as-SS Al-Zn alloys decreased with increased Zn contents, and as-SS Al-20Zn alloy showed a high impact toughness of 58 kJ/m^2.

Acknowledgments

This work was funded by the Research Program of Science and Technology of Guangxi (No. GKAB16380021), the Guangxi "Bagui" Teams for Innovation, Educational Commission of

Guangxi of China (No. KY2015ZD050), and Collaborative Innovation Center for Exploration of Hidden Nonferrous Metal Deposits and Development of New Materials in Guangxi.

References

1. I. Černý, J. Sís, and D. Mikulová, Short Fatigue Crack Growth in an Aircraft Al-Alloy of a 7075 Type After Shot Peening, *Surf. Coat. Technol.*, 2014, **243**(12), p 20–27
2. Ł. Kaczmarek, M. Stegliński, J. Sawicki, J. Świniarski, D. Batory, K. Kyzioł, Ł. Kołodziejczyk, W. Szymański, P. Zawadzki, and D. Kottfer, Optimization of the Heat Treatment and Tribological Properties of 2024 and 7075 Aluminium Alloys, *Arch. Metall. Mater.*, 2013, **58**(2), p 535–540
3. K. Kyzioł, K. Koper, M. Środa, M. Klich, and Ł. Kaczmarek, Influence of Gas Mixture during N^+ Ion Modification Under Plasma Conditions on Surface Structure and Mechanical Properties of Al-Zn Alloys, *Surf. Coat. Technol.*, 2015, **278**(6), p 30–37
4. K. Bewilogua, G. Bräuer, A. Dietz, J. Gäbler, G. Goch, B. Karpuschewski, and B. Szyszka, Surface Technology for Automotive Engineering, *CIRP Ann. Manuf. Technol.*, 2009, **58**(2), p 608–627
5. S.L. Pramod, A.K. Prasada Rao, B.S. Murty, and S.R. Bakshi, Effect of Sc Addition on the Microstructure and Wear Properties of A356 Alloy and A356-TiB_2 In Situ Composite, *Mater. Des.*, 2015, **78**, p 85–94
6. W.D. Zhang, Y. Liu, J. Yang, J.Z. Dang, H. Xu, and Z.M. Du, Effects of Sc Content on the Microstructure of As-Cast Al-7wt.% Si Alloys, *Mater. Charact.*, 2012, **66**, p 104–110
7. J.J. Wang, Z.M. Zhang, A.B. Phillion, S.Z. Shang, and G.M. Lu, Alloy Development and Reheating Process Exploration of Al-Si Casting Alloys with Globular Grains for Thixoforming, *J. Mater. Res.*, 2016, **31**(16), p 2482–2492
8. Y. Zheng, W.L. Xiao, S.J. Ge, W.T. Zhao, S.J. Hanada, and C.L. Ma, Effects of Cu Content and Cu/Mg Ratio on the Microstructure and Mechanical Properties of Al-Si-Cu-Mg Alloys, *J. Alloys Compd.*, 2015, **649**, p 291–296
9. R. Chen, Q.Y. Xu, H.T. Guo, Z.Y. Xia, Q.F. Wu, and B.C. Liu, Modeling the Precipitation Kinetics and Tensile Properties in Al-7Si-Mg Cast Aluminum Alloys, *Mater. Sci. Eng. A*, 2017, **685**, p 403–416
10. T.B. Massalski, *Alloy Phase diagrams*, Materials Park, OH, ASM International, 1993, p 239
11. X. Sauvage, M.Y. Murashkin, B.B. Straumal, E.V. Bobruk, and R.Z. Valiev, Ultrafine Grained Structures Resulting from SPD-Induced Phase Transformation in Al-Zn Alloys, *Adv. Eng. Mater.*, 2015, **17**(12), p 1821–1827
12. A.A. Mazilkin, B.B. Straumal, E. Rabkin, B. Baretzky, S. Enders, S.G. Protasova, O.A. Kogtenkova, and R.Z. Valiev, Softening of Nanostructured Al-Zn and Al-Mg Alloys After Severe Plastic Deformation, *Acta Mater.*, 2006, **54**(15), p 3933–3939
13. N.Q. Chinh, P. Jenei, J. Gubicza, E.V. Bobruk, R.Z. Valievb, and T.G. Langdon, Influence of Zn Content on the Microstructure and Mechanical Performance of Ultrafine-Grained Al-Zn Alloys Processed by High-Pressure Torsion, *Mater. Lett.*, 2017, **186**, p 334–337
14. W.B. Zhou, C.Y. Liu, P.F. Yu, B. Zhang, Z.Y. Ma, K. Luo, M.Z. Ma, and R.P. Liu, Effect of Scandium on Microstructure and Mechanical Properties of High Zinc Concentration Aluminum Alloys, *Mater. Charact.*, 2017, **127**, p 371–378
15. S.S. Shin, K.M. Lim, and I.M. Park, Characteristics and Microstructure of Newly Designed Al-Zn-Based Alloys for the Die-Casting Process, *J. Alloys Compd.*, 2016, **671**, p 517–526
16. C.Y. Liu, B. Qu, Z.Y. Ma, M.Z. Ma, and R.P. Liu, Recrystallization, Precipitation, and Resultant Mechanical Properties of Rolled Al-Zn Alloy After Aging, *Mater. Sci. Eng. A*, 2016, **657**, p 284–290
17. C.Y. Liu, M.Z. Ma, R.P. Liu, and K. Luo, Evaluation of Microstructure and Mechanical Properties of Al-Zn Alloy During Rolling, *Mater. Sci. Eng. A*, 2016, **654**, p 436–441
18. C.Y. Liu, L. Yu, M.Z. Ma, R.P. Liu, and Z.Y. Ma, Dynamic Precipitation of Al-Zn Alloy During Rolling and Accumulative Roll Bonding, *Philos. Mag. Lett.*, 2015, **95**(11), p 539–546
19. C.Y. Liu, H.J. Jiang, C.X. Wang, H.Q. Qi, Y.B. Li, M.Z. Ma, and R.P. Liu, Static and Dynamic Precipitation Behavior of the Al-20wt.% Zn Alloy, *Chin. Phys. Lett.*, 2016, **33**(5), p 056101
20. C.Y. Liu, B. Zhang, P.F. Yu, R. Jing, M.Z. Ma, and R.P. Liu, Microstructures and Mechanical Properties of Al/Zn Composites Prepared by Accumulative Roll Bonding and Heat Treatment, *Mater. Sci. Eng. A*, 2013, **580**, p 36–40
21. C.Y. Liu, M.Z. Ma, R.P. Liu, L. Yu, and K. Luo, Effect of Zn Particles on Ductility of the Accumulative Roll-Bonding Composites, *Sci. China Phys. Mech. Astron.*, 2015, **58**(10), p 104601
22. B. Dang, C.C. Liu, F. Liu, Y.Z. Liu, and Y.B. Li, Effect of As-Solidified Microstructure on Subsequent Solution-Treatment Process for A356 Al Alloy, *Trans. Nonferrous Metal Soc. China*, 2016, **26**(3), p 634–642
23. S. Meenia, F. Khan, S. Babu, R.J. Immanuel, and S.K. Panigrahi, Particle Refinement and Fine-Grain Formation Leading to Enhanced Mechanical Behaviour in a Hypo-Eutectic Al-Si Alloy Subjected to Multi-pass Friction Stir Processing, *Mater. Charact.*, 2016, **113**, p 134–143
24. W.M. Jiang, Z.T. Fan, X. Chen, B.J. Wang, and H.B. Wu, Combined Effects of Mechanical Vibration and Wall Thickness on Microstructure and Mechanical Properties of A356 Aluminum Alloy Produced by Expendable Pattern Shell Casting, *Mater. Sci. Eng. A*, 2014, **619**, p 228–237
25. C.Y. Liu, Q. Wang, Y.Z. Jia, B. Zhang, R. Jing, M.Z. Ma, Q. Jing, and R.P. Liu, Effect of W Particles on the Properties of Accumulatively Roll-Bonded Al/W Composites, *Mater. Sci. Eng. A*, 2012, **547**, p 120–124
26. C.Y. Liu, Q. Wang, Y.Z. Jia, B. Zhang, R. Jing, M.Z. Ma, Q. Jing, and R.P. Liu, Evaluation of Mechanical Properties of 1060-Al Reinforced with WC Particles via Warm Accumulative Roll Bonding Process, *Mater. Des.*, 2013, **43**, p 367–372
27. C.Y. Liu, P.F. Yu, X.Y. Wang, M.Z. Ma, and R.P. Liu, Preparation of High-Strength Al-Mg-Si-Cu-Fe Alloy via Heat Treatment and Rolling, *Int. J. Miner. Met. Mater.*, 2014, **21**(7), p 702–710
28. D.F. Li, C.X. Cui, X. Wang, Q.Z. Wang, C. Chen, and S.Q. Liu, Microstructure Evolution and Enhanced Mechanical Properties of Eutectic Al-Si Die Cast Alloy by Combined Alloying Mg and La, *Mater. Des.*, 2016, **90**, p 820–828
29. K. Natori, H. Utsunomiya, and T. Tanaka, Improvement in Formability of Semi-Solid Cast Hypoeutectic Al-Si Alloys by Equal-Channel Angular Pressing, *J. Mater. Process. Technol.*, 2017, **240**, p 240–248